The Astrophysical Journal, 1000:115 (9pp), 2026 March 20 https://doi.org/10.3847/1538-4357/ae47ea

Constraining the Fraction of LIGO/Virgo/KAGRA Binary Black Hole Merger Events Associated with Active Galactic Nucleus Flares

Liang-Gui Zhu (朱良贵)[1,2], Lei He (贺雷)[1,2], Xian Chen (陈弦)[3,4], and Wen Zhao (赵文)[1,2]
[1] Department of Astronomy, University of Science and Technology of China, Hefei, Anhui 230026, People's Republic of China; lianggui.zhu@ustc.edu.cn, helei0831@mail.ustc.edu.cn, wzhao7@ustc.edu.cn
[2] School of Astronomy and Space Sciences, University of Science and Technology of China, Hefei, Anhui 230026, People's Republic of China
[3] Department of Astronomy, School of Physics, Peking University, Beijing 100871, People's Republic of China; xian.chen@pku.edu.cn
[4] Kavli Institute for Astronomy and Astrophysics, Peking University, Beijing 100871, People's Republic of China
Received 2026 January 13; revised 2026 February 6; accepted 2026 February 17; published 2026 March 17

Abstract

The formation channels of binary black hole (BBH) mergers detected by the LIGO/Virgo/KAGRA network remain uncertain. BBH mergers occurring inside the disks of active galactic nuclei (AGNs) may interact with surrounding gas and generate observable optical flares. We test this scenario by quantifying the spatial and temporal correlation between BBH events in GWTC-4.0 and AGN flares identified from six years of the Zwicky Transient Facility (ZTF) DR23 data. Using 80 BBH mergers selected for adequate localization, redshift reach, observing-epoch overlap, and ZTF sky coverage, we construct a likelihood for the flare-associated fraction, $f_{\rm flare}$, that combines each event's 3D localization with a locally estimated flare number density derived from a 3D Voronoi tessellation, while explicitly accounting for survey boundaries and incomplete catalog coverage. Adopting a postmerger time window of 200 days for potential counterparts, we infer $f_{\rm flare} = 0.07^{+0.24}_{-0.05}$ (90% confidence level). This nonzero maximum-likelihood value is driven primarily by GW190412, for which a single flare candidate (J143041.67+355703.8) is consistent in both time and spatial position. The candidate's light curve is limited to two data points during its peak, so it remains classified only as a candidate AGN flare. Excluding GW190412 yields results consistent with no association and an upper limit of $f_{\rm flare} < 0.17$ at 90% confidence level. The intrinsic properties of GW190412 and the characteristics of the candidate host AGN are broadly consistent with theoretical expectations for the AGN-disk formation channel, motivating continued, targeted electromagnetic follow-up of well-localized and highly asymmetric BBH mergers in current and upcoming time-domain surveys.

Unified Astronomy Thesaurus concepts: Gravitational wave sources (677); Black holes (162); Active galactic nuclei (16); Optical flares (1166); Sky surveys (1464)

1. Introduction

The LIGO/Virgo/KAGRA (LVK) ground-based gravitational-wave (GW) detector network has officially released version 4.0 of the Gravitational-Wave Transient Catalog (GWTC-4.0; A. G. Abac et al. 2025a; LVK Collaboration et al. 2025b). This catalog presents 176 compact binary coalescence events with parameter estimates (false alarm rate $<1\,{\rm yr}^{-1}$), covering observations from the first observing run (O1) through the first part of the fourth observing run (O4a; B. P. Abbott et al. 2019a; R. Abbott et al. 2021, 2023, 2024). More than 90% of the reported events originate from binary black hole (BBH) mergers. The properties of these BBH events have substantially advanced our understanding of stellar-mass black hole (BH) and BBH populations (e.g., B. P. Abbott et al. 2016, 2019b; R. Abbott et al. 2020a, 2020b, 2020c; A. G. Abac et al. 2025b, 2025c; LVK Collaboration et al. 2025c). However, the origins of the observed BBHs remain highly uncertain.

Several formation channels have been proposed, including the evolution of primordial black holes (S. W. Hawking 1974; E. Bagui et al. 2025), remnants of Population III stars (A. Stacy et al. 2010; S. Hirano & V. Bromm 2017), and isolated binary evolution in galactic fields (H. A. Bethe & G. E. Brown 1998; K. Belczynski et al. 2002; M. Dominik et al. 2012; K. A. Postnov & L. R. Yungelson 2014; S. E. Woosley 2016; L. du Buisson et al. 2020). Alternatively, BBHs may form dynamically through hierarchical mergers in dense environments, such as young stellar clusters (B. M. Ziosi et al. 2014; S. Banerjee 2017; U. N. Di Carlo et al. 2019), globular clusters (M. C. Miller & D. P. Hamilton 2002; M. Colpi et al. 2003; C. L. Rodriguez et al. 2015, 2016; G. Fragione & B. Kocsis 2018), nuclear star clusters (F. Antonini & F. A. Rasio 2016; F. Antonini et al. 2019), and the disks of active galactic nuclei (AGNs; B. McKernan et al. 2012; I. Bartos et al. 2017b; Y. Yang et al. 2019a; H. Tagawa et al. 2020b). Each proposed channel is theoretically capable of producing a subset of the detected BBH events (T. Kinugawa et al. 2021; B. Liu & D. Lai 2021; Y.-J. Li et al. 2024b; G.-P. Li & X.-L. Fan 2025a). However, the predicted distributions of intrinsic BBH properties exhibit significant overlap across channels, despite their distinct characteristic features. This degeneracy, coupled with the insufficient precision of GW source localization (for identifying the unique host of a GW source), poses a significant challenge to identifying the formation pathways of individual BBH events (e.g., V. De Luca et al. 2025; V. Delfavero et al. 2025; Y.-J. Li et al. 2025a; S. Liu et al. 2025; G.-P. Li & X.-L. Fan 2025b; L. Passenger et al. 2025; A. Tanikawa et al. 2025). Consequently, this challenge necessitates relying on population-level statistical methods to infer BBH formation channels, namely, estimating the fractional contribution of each proposed channel to the overall observed BBH population.

Currently proposed methods for such inference include: (i) hierarchical Bayesian inference (T. J. Loredo 2004; M. Fishbach et al. 2018; I. Mandel et al. 2019; E. Thrane & C. Talbot 2019), (ii) spatial correlation tests between BBHs and AGNs (J. Braun et al. 2008; I. Bartos et al. 2017a; N. Veronesi et al. 2022, 2023, 2025), and (iii) spatial correlation tests between BBHs and electromagnetic (EM) transients (e.g., flares, N. Veronesi et al. 2024) (also see A. Palmese et al. 2021, with similar principles but a different statistical framework). The first method quantifies the consistency between the observed posterior distributions of BBH source parameters (e.g., component masses, mass ratios, spins, effective spins, and orbital eccentricities; M. Mapelli 2021; M. Mapelli et al. 2021; F. Santoliquido et al. 2021; M. Zevin et al. 2021; G.-P. Li et al. 2023; E. Berti et al. 2025) and the predicted distributions from theoretical formation channels. Its key advantage lies in not relying on additional observational data, but the results are highly sensitive to the accuracy of the theoretical models themselves (B. P. Abbott et al. 2019b; V. Gayathri et al. 2021; Y.-Z. Wang et al. 2021b, 2022; Y.-J. Li et al. 2024a; G.-P. Li & X.-L. Fan 2025a; LVK Collaboration et al. 2025c).

The second method is specifically designed to test the AGN formation channel for BBHs (I. Bartos et al. 2017a). AGN disks are considered a favorable environment for producing LVK BBH events due to several key characteristics (I. Bartos et al. 2017b; Y. Yang et al. 2019a; H. Tagawa et al. 2020b; M. Cantiello et al. 2021; V. Gayathri et al. 2021): a number density of compact objects far exceeding that in galactic nuclear star clusters; dense gas that can fuel BH growth via accretion; and gas-induced dynamical friction, which promotes the efficient formation of bound multi-BH systems, enhances merger rates, and leads to spontaneous spin alignment, even for BBHs with distinctive properties such as larger masses, smaller mass ratios, higher premerger spins, higher effective inspiral spin magnitudes, and greater eccentricities (Y. Yang et al. 2019b; H. Tagawa et al. 2020a, 2021; J. Samsing et al. 2022; Y.-J. Li et al. 2025b, 2025c). Using this method, L.-G. Zhu & X. Chen (2025) reported preliminary evidence for a statistical association between LVK GW events and AGNs.

The third method extends the second by further restricting the spatial correlation targets to AGNs that exhibit temporally coincident EM transients (N. Veronesi et al. 2024). Within the framework of general relativity, BBH mergers in vacuum do not produce EM emission. However, if a BBH merger occurs within an AGN disk, the interaction of its component black holes—and the remnant black hole—with the surrounding gas before and after the merger can potentially generate observable EM counterparts (B. McKernan et al. 2019; S. S. Kimura et al. 2021; J.-M. Wang et al. 2021a; K. Chen & Z.-G. Dai 2024; J. C. Rodríguez-Ramírez et al. 2024). The confirmed spatial correlation between a fraction of BBH mergers and such AGN EM transients can be interpreted as evidence that those BBHs formed in AGN disks.

N. Veronesi et al. (2024) first applied the third method to statistically test the spatial correlation between BBH events detected during the third LVK observing run and candidate AGN flares identified from the Zwicky Transient Facility (ZTF) data by M. J. Graham et al. (2023), finding no evidence for an association (a result also supported by T. Cabrera et al. (2025) using a different framework). However, observations from other studies provide some support for the possibility that a subset of BBH mergers may be accompanied by flare counterparts. For instance, M. J. Graham et al. (2020) reported a high-confidence AGN flare counterpart associated with GW190521 (see A. Palmese et al. (2021) for a detailed analysis), and later works (T. Cabrera et al. 2024; L. He et al. 2025a, 2025b; H. Zhang et al. 2025) have identified other candidate AGN flares potentially correlated with other BBH mergers. The nondetection of N. Veronesi et al. (2024) is likely attributable to the low completeness of the flare catalog used.

In this work, we employ updated observational data and an improved statistical framework to analyze the spatial correlation between LVK BBH mergers and candidate flares, thereby inferring the fraction of detected BBH merger events with associated flare counterparts. The enhanced completeness of the updated dataset increases the probability of capturing genuine EM counterparts, while the refined method more effectively accounts for spatial anisotropy in the flare catalog, reducing potential systematic biases.

This paper is organized as follows. Section 2 describes the data, Section 3 introduces the statistical framework, Section 4 presents the findings, and Section 5 provides the discussion. We adopt a flat ΛCDM cosmology ($H_0 = 67.8\,\mathrm{km\,s^{-1}\,Mpc^{-1}}$, $\Omega_M = 0.308$; P. A. R. Ade et al. 2016) for redshift–distance conversion throughout this work.

2. Data

The data used in this work consist of skymaps of BBH GW sources and AGN flare catalogs. The skymaps of BBH sources are obtained from the results of GWTC-4.0 of the LVK Collaboration, including the officially published BBH events from the first observing run to the first part of the fourth observing run (O1–O4a; B. P. Abbott et al. 2019a; R. Abbott et al. 2021, 2023, 2024; LVK Collaboration et al. 2025b).[5] These skymaps provide us with the probability density distribution function of the three-dimensional (3D) localization of each BBH source.

The AGN flare catalog used in this work is adopted from L. He et al. (2026). This catalog was constructed by searching six years (2018 March–2024 October) of data from the ZTF (E. C. Bellm et al. 2019; M. J. Graham et al. 2019).[6] L. He et al. (2026) provide two versions: a refined AGN flare catalog (AGNFRC) containing ∼2000 high-confidence flares, and a coarse AGN flare catalog (AGNFCC) containing ∼28,000 candidate flares. Both were identified using Bayesian blocks and Gaussian processes, with the AGNFRC being a subset of the AGNFCC. Given the still limited understanding of the observational characteristics of genuine BBH merger-associated flares, we utilize the more complete AGNFCC to search for candidate counterparts in this work, after removing flares that have been identified as tidal disruption events, supernovae, and blazars from the catalog. The AGNFCC used covers approximately 55% of the sky.

To enhance computational efficiency, we applied a selection to the BBH events, retaining only those satisfying the following criteria for our analysis: (i) a spatial localization error volume ΔV_c smaller than $10^{10}\,\mathrm{Mpc^3}$, since poorer localization would cause the statistical signal of its unique

[5] GWTC-4.0 is available at: https://gwosc.org/eventapi/html/GWTC/.

[6] ZTF Data Release 23 is available at: https://www.ztf.caltech.edu/ztf-public-releases.html.

flare counterpart (if it exists) to be more easily drowned out by numerous flare candidates; (ii) a fraction of the 90% confidence level (CL) localization error volume covered by the flare catalog greater than 0.2, because a lower coverage fraction increases the probability that the true flare counterpart of the BBH event was missed observationally; (iii) the entire localization error volume lying within $z < 1.5$, a redshift range containing approximately 90% of the cataloged flares; and (iv) a merger time falling within the observational epoch of the ZTF data. In this work, we utilized a total of 80 BBHs from GWTC-4.0 that met these criteria. Our selection is independent of BBH intrinsic properties (and hence of formation channels), and the resulting subsample (representing ∼50% of the total) remains representative of the full population regarding potential flare associations.

3. Methodology

3.1. Statistical Framework

In this work, we adopt the statistical framework presented by L.-G. Zhu & X. Chen (2025) to test the spatial correlation between the LVK BBH events and ZTF flares. This framework was originally introduced by I. Bartos et al. (2017a) to assess spatial correlations between GWs and AGNs. It was later modified by N. Veronesi et al. (2023, 2024) to incorporate skymap information from GW events more effectively. L.-G. Zhu & X. Chen (2025) further extended the method by implementing a Voronoi tessellation approach to address the significant anisotropies in the AGN catalog. Given that the flare catalog used here also exhibits significant anisotropy, the framework of L.-G. Zhu & X. Chen (2025) is particularly well-suited for our analysis.

Let $f_{\rm flare}$ denote the fraction of BBH merger events consistent with the observed EM flares. For a dataset consisting of N BBH events, the likelihood can be expressed as

$$\mathcal{L}(f_{\rm flare}) = \prod_{i=1}^{N} [0.9 f_{{\rm c},i}\, f_{\rm flare}\, \mathcal{S}_i + (1 - 0.9 f_{{\rm c},i}\, f_{\rm flare})\mathcal{B}_i], \quad (1)$$

where $f_{{\rm c},i}$ represents the coverage fraction of the flare catalog for the localization error volume of the ith GW event, and the coefficient 0.9 comes from the CL employed in the skymaps of BBH events. The functions $\mathcal{S}_i$ and $\mathcal{B}_i$ represent the "signal probability" and "background probability," respectively. These probabilities are constructed on the following principle: the statistical expectation of $\mathcal{S}_i$ is greater than that of $\mathcal{B}_i$ if the ith BBH event is consistent with an observed flare and vice versa. A theoretical proof provided in the appendix of L.-G. Zhu & X. Chen (2025) demonstrates that an unbiased estimate of $f_{\rm flare}$ can be achieved using the likelihood form of Equation (1).

The signal probability is defined as

$$\mathcal{S}_i = \sum_{j=1}^{N_{\rm flare}} \frac{p_i(\mathbf{x}_j)}{n_{\rm flare}(\mathbf{x}_j)}, \quad (2)$$

where $\mathbf{x}_j$ denotes the 3D position of the jth candidate flare, $p_i(\mathbf{x}_j)$ represents the spatial localization probability density of the ith BBH event at position $\mathbf{x}_j$, $n_{\rm flare}(\mathbf{x}_j)$ represents the spatial number density of the jth candidate flare, and $N_{\rm flare}$ is the total number of candidate flares of the BBH event. The search for the candidate flares requires spatial and temporal coincidence with the BBH event: (i) located within the 90% CL error volume of the BBH event; (ii) the start time of the rise and the peak time of the flare both occur within 200 days after the BBH merger. The experimental search window was set based on the EM flare production model of ram pressure stripping (B. McKernan et al. 2019); when the time delay of the flare counterpart for a BBH merger GW event falls within this window, the flare is more likely to be observable. This search window aligns with previous researches (M. J. Graham et al. 2020, 2023; N. Veronesi et al. 2024).

To derive $n_{\rm flare}$ as a function of $\mathbf{x}_j$, we follow L.-G. Zhu & X. Chen (2025) and apply a 3D first-order Voronoi tessellation method (G. Voronoi 1908; A. Okabe et al. 1992; K. A. Brakke 2005; V. Lucarini 2009; I. Vavilova et al. 2021). Since the Voronoi tessellation is suitable for large samples, we first select all flares that are temporally consistent with each utilized BBH event from the total flare catalog according to the criteria for searching for candidate flare counterparts of BBHs outlined by M. J. Graham et al. (2023): (i) the start time of the Gaussian rise ($t_0 - 1.8t_{\rm g}$) and the peak time t_0 of the flare occur within 200 days after the BBH merger, (ii) the timescale $t_{\rm g}$ of Gaussian rise of the flare is $t_{\rm g} \leqslant 100$ days, and (iii) the exponential decay timescale $t_{\rm e}$ of the flare is $t_{\rm e} \leqslant 200$ days. These flares form a subcatalog; we then use the Voronoi tessellation method to partition the comoving volume covered by the flare subcatalog into polyhedral cells within a Cartesian coordinate system, with each cell containing exactly one flare. The flare density is equal to the reciprocal of the volume of the Voronoi polyhedron cell, i.e., $n_{\rm flare}(\mathbf{x}_j) = 1/V_{\rm cell}(\mathbf{x}_j)$.

The background probability $\mathcal{B}_i$ is defined as the expected value of $\mathcal{S}_i$ when the BBH event is unrelated to all observed candidate flares. Because $\mathcal{S}_i$ merely performs a summation over the probability density distribution of BBH source spatial localization using observed flare samples, and flare catalogs are often incomplete—potentially covering only a portion of the localization error volume of the BBH event—the definition of $\mathcal{B}_i$ must account for this limitation. The background probability can be expressed as

$$\mathcal{B}_i = 0.9 f_{{\rm c},i}. \quad (3)$$

The coverage fraction can be calculated from

$$f_{{\rm c},i} = \frac{1}{\mathcal{N}_{\rm CL}} \iiint_{\Delta V_{\rm c,flare}} p_i(\alpha, \delta, D_{\rm c}) |J|\, d\alpha\, d\delta\, dD_{\rm c}, \quad (4)$$

where (α, δ) are celestial coordinates, $D_{\rm c}$ is the comoving distance, $p_i(\alpha, \delta, D_{\rm c})$ represents the spatial probability density distribution of the ith BBH source localization, $|J| \equiv D_{\rm c}^2 \cos\delta$ is the Jacobian determinant for spherical-to-Cartesian coordinate transformation, and $\mathcal{N}_{\rm CL} = 0.9$ is the normalization factor that accounts for the 90% CL localization error volume. The integration domain $\Delta V_{\rm c,flare}$ is the portion of the 90% CL localization volume of the ith BBH event that is covered by the union of the Voronoi cells associated with all flares used in the analysis.

3.2. Accounting for the Boundary Effects

An examination of the likelihood formula in Equation (1) reveals a complete degeneracy between the parameters $f_{{\rm c},i}$ and

$f_{\rm flare}$. Consequently, the reliability of estimating $f_{\rm flare}$ depends directly on the accuracy of the $\{f_{{\rm c},i}\}$ calculations. For the majority of GW events in our sample—those whose localization error volume is only partially covered by the flare catalog—the calculation of $f_{{\rm c},i}$ is highly sensitive to the adopted sky-coverage boundaries. Therefore, it is essential to rigorously account for boundary effects in the data analysis.

To accurately account for boundary effects, we performed two data-processing steps. First, we employed the alphashape algorithm to determine the sky-coverage boundaries of the flare distribution from the full flare catalog, excluding isolated flares and small-scale clusters located outside these boundaries. When calculating the volumes of the polyhedral cells (occupied by flares) using the Voronoi tessellation method, we removed vertices lying outside the sky boundaries (including those with redshifts exceeding the maximum threshold of $z = 1.5$). This procedure ensures that all Voronoi polyhedral cells reside within the sky boundaries and possess finite volumes. However, at this stage, the outer surfaces of the resulting polyhedral tessellations (formed by the retained flares) do not coincide with the original sky boundaries. This discrepancy becomes more pronounced in regions of lower flare spatial density. The volumes enclosed by these polyhedral tessellation surfaces define the precise integration region, $\Delta V_{\rm c,flare}$, for calculating the coverage fraction $f_{{\rm c},i}$ in Equation (4).

Second, to precisely determine the volumes occupied by the polyhedral tessellations, we discretize the total volume (enclosed by the sky boundaries) into numerous minute cubic elements within the comoving-distance space. Each element is labeled by the coordinates of its center. The volume of each Voronoi polyhedral cell (associated with a flare) is then determined by employing the scipy.spatial.Delaunay algorithm to select all cubic elements whose centers lie inside that cell. The union of these selected elements defines the integration region for calculating $f_{{\rm c},i}$. Note that the computational precision of $f_{{\rm c},i}$ depends critically on the size of the cubic elements, which must be chosen to be much smaller than the volume of the smallest Voronoi cell in the sample.

4. Results

4.1. Indications of a Nonzero $f_{\rm flare}$

We first employ a postmerger search window of 200 days and the condition ($t_{\rm g} \leqslant 100$ days, $t_{\rm e} \leqslant 200$ days) to identify all flares temporally coincident with LVK BBH events from AGNFCC. The fraction of BBHs associated with flares, $f_{\rm flare}$, is estimated using Equation (1), and the resulting estimates are presented in Figure 1.

The key distinction between our estimates and those from previous studies (e.g., N. Veronesi et al. 2024; T. Cabrera et al. 2025) is the detection of a nonzero best-fit value for $f_{\rm flare}$. We estimate $f_{\rm flare} = 0.07^{+0.24}_{-0.05}$ (maximum-likelihood value with symmetric 90% CLs, see the red solid curve in Figure 1). This result provides the first statistically derived preliminary evidence that a fraction of BBH merger events are accompanied by observable EM flares, representing a significant step forward since the search for candidate flares for the GW190521 event was reported by M. J. Graham et al. (2020).

Before drawing a definitive conclusion, we investigated the origin of the signal for this nonzero $f_{\rm flare}$ evidence. We examined the signal probability $\mathcal{S}_i$ for each individual BBH event, as a higher $\mathcal{S}_i$ provides stronger support for $f_{\rm flare} > 0$.

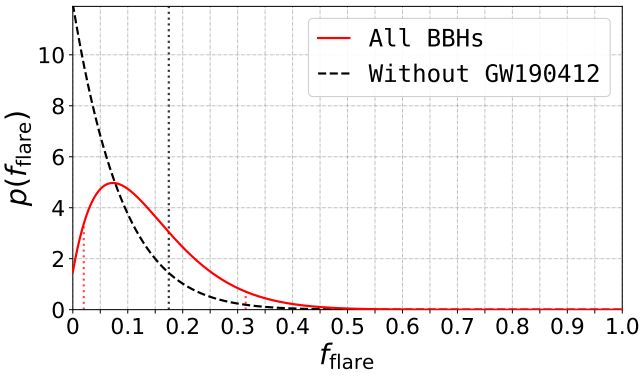

Figure 1. Probability density distributions of $f_{\rm flare}$ derived from the LVK GWTC-4.0 BBH events and the ZTF AGN candidate flares. The red solid and black dashed curves represent the results derived from the all BBH events and the set without GW190412, respectively. The vertical red and black dotted lines indicate the error interval and the upper limit at the 90% CL, correspondingly.

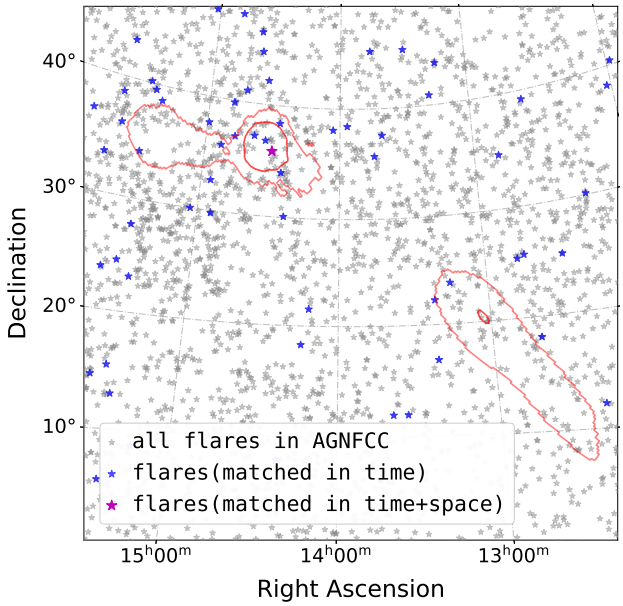

Figure 2. Skymap of GW190412 event and candidate flares. The red contours represent the 50% and 90% CL sky localization regions. The gray, blue, and purple star points denote all flares in AGNFCC, those consistent with GW190412 in time, and those consistent in both time and spatial localization (sky position + distance), correspondingly.

We found that GW190412 has an exceptionally high signal probability of $\mathcal{S}_i > 10$, which far exceeds those of the other BBH events. After removing it, the estimated $f_{\rm flare}$ becomes consistent with zero (black dashed curve in Figure 1), with an upper limit of 0.17 at the 90% CL, in agreement with the result from N. Veronesi et al. (2024). This evidence of $f_{\rm flare} > 0$ is primarily driven by GW190412.

However, this does not imply that the preliminary evidence we obtained for $f_{\rm flare} > 0$ is unreliable. Figure 2 presents the skymap of GW190412 localization and the distribution of flares from AGNFCC. The gray points represent all AGNFCC flares, the blue points mark flares temporally coincident with the GW190412 merger, and the purple point identifies the sole candidate: J143041.67+355703.8, consistent with the GW190412 merger in both time and spatial position. A number of gray points and several blue points fall within the sky localization region of GW190412, indicating that the

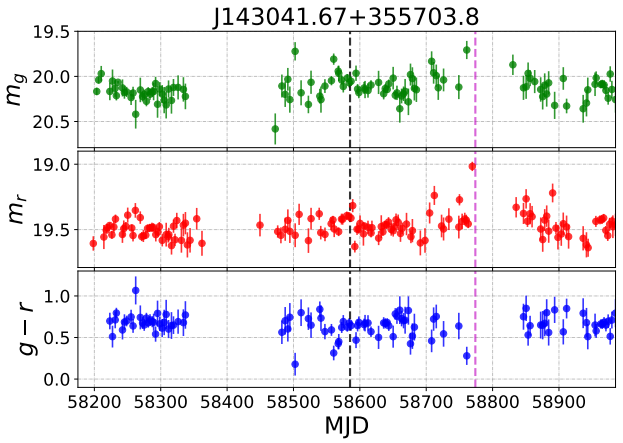

Figure 3. The ZTF g- and r-band light curves for the J143041.67+355703.8 candidate flare associated with GW190412. The green and red points (with error bars) show the g- and r-band apparent magnitudes, respectively; the blue points denote the $g-r$ color. The vertical black and magenta dashed lines mark the merger time of GW190412 and the candidate flare's peak time, respectively.

survey coverage of AGNFCC was relatively complete across this sky area during the merger epoch. This suggests that the high signal probability derived from the J143041.67+355703.8 candidate flare is unlikely to be merely an artifact of residing in an underdense region (or "cavity") of the flare distribution, where a low local flare density $n_{\rm flare}$ would lead to an artificially high signal probability $\mathcal{S}_i$ (see Equation (2)).

Additionally, among the 80 BBH events used in this work, we find that 12 have localization error volumes comparable to or smaller than that of GW190412 (within a factor of 3). Within this subset, eight events exhibit a signal probability of zero, and the average ratio of signal probability to background probability is close to unity. This indicates that although the signal probability of GW190412 itself is an outlier, the overall distribution of signal probabilities for events with similarly precise localizations is statistically consistent with a balanced population.

4.2. Light Curve and Host AGN Properties of the Candidate Flare Counterpart for GW190412

The light curve of the J143041.67+355703.8 candidate flare of GW190412 is shown in Figure 3. When fitting the light curve using an empirical form

$$y(t)=\begin{cases} r_0+A\exp\left[-\frac{(t-t_0)^2}{2t_{\rm g}^2}\right], & t\leqslant t_0 \\ r_0+A\exp\left[-\frac{(t-t_0)}{t_{\rm e}}\right], & t>t_0, \end{cases} \quad (5)$$

the best-fit timescales of Gaussian rise and exponential decay are $t_{\rm g}=3$ days and $t_{\rm e}=24$ days, respectively, with the fitted reference flare peak time t_0, amplitude A, and background flux r_0. The time delay between the merger of the GW190412 event and the peak of the J143041.67+355703.8 candidate flare is about 189 days. As can be seen from Figure 3, there is unfortunately only one observational data point in each of the g and r bands around the peak time of the J143041.67+355703.8 candidate flare, corresponding to a magnitude variation of ∼0.5 mag. Although the probability of J143041.67+355703.8 being a genuine flare, estimated using the test statistic for flare searches employed by L. He et al. (2026), reaches $p_{\rm flare}>0.99$, it is still insufficient to draw a strong conclusion comparable to that of M. J. Graham et al. (2020).

We specifically note that the peak data point of the J143041.67+355703.8 candidate flare corresponds to the final observation in a contiguous ZTF monitoring block for this source. A manual inspection of hundreds of ZTF light curves of flares in the AGNFCC reveals that a rising trend in the final data points of a continuous observing block is relatively common. This phenomenon may be attributed to systematic photometric biases when the source is observed at low elevation, as it approaches the limit of ZTF's observable window at the end of a block. Nevertheless, a brightening as large as ∼0.5 mag, as seen for J143041.67+355703.8, remains rare. Furthermore, based on the spatial localization volume of GW190412 ($\bar{z}\approx0.15$, $\Delta V_{\rm c}\approx10^7\,{\rm Mpc}^3$, R. Abbott et al. 2020b), the average number density of AGNFCC flares ($\sim0.4\times10^{-7}\,{\rm Mpc}^{-3}$ per 200 days, derived from ∼6400 flares with $z<0.5$ out of a total comoving volume of $1.7\times10^{10}\,{\rm Mpc}^3$), we estimate that the number of flares ZTF could expect to detect within GW190412's error volume is ∼0.4. This implies that the probability of finding at least one candidate flare from the AGNFCC that matches the GW190412 skymap by pure chance reaches $\gtrsim$33%.

To further investigate whether the GW190412 event and J143041.67+355703.8 candidate flare share a common origin, we examined the properties of the GW190412 source and the J143041.67+355703.8 candidate flare's host AGN. The inferred intrinsic parameters of the GW190412 event, which may indicate its formation channel, are as follows (R. Abbott et al. 2020b, 2021): (i) source-frame mass of the more massive BH $m_1=30.1^{+4.6}_{-5.3}\,M_\odot$, (ii) mass ratio $q\equiv m_2/m_1=0.28^{+0.12}_{-0.07}$, (iii) dimensionless spin magnitudes of component BHs ($\chi_1=0.44^{+0.16}_{-0.22}$, $\chi_2\sim0.5^{+0.4}_{-0.4}$), (iv) effective inspiral spin parameter $\chi_{\rm eff}=0.25^{+0.08}_{-0.11}$, and (v) formation eccentricity $e_{\rm f}\sim0.34^{+0.53}_{-0.29}$ (V. Baibhav 2025). The extreme mass ratio, nonzero premerger spins, and formation eccentricity in GW190412 suggest that it likely formed through a hierarchical merger channel (U. N. Di Carlo et al. 2020; D. Gerosa et al. 2020; C. L. Rodriguez et al. 2020; ; A. Olejak et al. 2020; B. Liu & D. Lai 2021). Its nonzero effective spin further supports an origin in an AGN environment (Y. Yang et al. 2019b; A. Secunda et al. 2020; H. Tagawa et al. 2020a, 2021; V. Gayathri et al. 2021).

Regarding the host AGN of the J143041.67+355703.8 candidate flare, its apparent B-band magnitude is recorded as 21.04 mag (E. W. Flesch 2023). Adopting a typical bolometric correction of $L_{\rm bol}/L_B\approx16$ for a bolometric luminosity of $\sim10^{43}\,{\rm erg\,s^{-1}}$ (P. F. Hopkins et al. 2007; X. Shen et al. 2020), we roughly estimate its bolometric luminosity to be $L_{\rm bol}\approx3.3\times10^{43}\,{\rm erg\,s^{-1}}$. Furthermore, based on the host AGN spectrum from the first data release of the Dark Energy Spectroscopic Instrument (DESI; DESI Collaboration et al. 2025), we estimate the mass of its central massive BH to be $M_{\rm MBH}\approx10^7\,M_\odot$ (see the Appendix for the spectrum of the J143041.67+355703.8 flare's host AGN). From $L_{\rm bol}$ and $M_{\rm MBH}$, the Eddington ratio of the host AGN is estimated as $\lg\lambda_{\rm Edd}\approx-1.6$, a value lower than that of 70% of AGNs with $L_{\rm bol}<10^{45}\,{\rm erg\,s^{-1}}$ presented by Q. Wu & Y. Shen (2022). The relatively lower $L_{\rm bol}$ and lower $\lambda_{\rm Edd}$ of the host AGN of J143041.67+355703.8 are consistent with the property constraints reported for AGNs that host BBHs

(L.-G. Zhu & X. Chen 2025). They also match the characteristic AGN properties predicted by theoretical studies (e.g., E. Grishin et al. 2024; S. Gilbaum et al. 2025) that suggest the presence of migration traps for BHs in AGN disks.

In summary, the intrinsic parameters of the GW and the properties of the flare's host AGN collectively support an association between the BBH merger GW190412 and the candidate flare J143041.67+355703.8. We note, however, that the ZTF obtained only two observations during the candidate flare's peak phase. We have also searched for the J143041.67+355703.8 flare in data from other transient surveys, including the Transient Name Server (TNS), the Asteroid Terrestrial-impact Last Alert System (ATLAS; J. L. Tonry et al. 2018), and the All-Sky Automated Survey for Supernovae (ASAS-SN; K. Hart et al. 2023). Similarly, no effective observations are available from these archives during the candidate flare's peak period.

5. Discussion

In this work, we estimate the fraction of the LVK BBH merger events that are associated with AGN flares observed by ZTF. Our preliminary result suggests that $f_{\rm flare} = 0.07^{+0.24}_{-0.05}$ of BBH mergers may have an associated ZTF flare. However, this nonzero $f_{\rm flare}$ is primarily contributed by the association between the GW190412 event and the J143041.67+355703.8 candidate flare. Despite ZTF having only two effective observations during the peak period of the J143041.67+355703.8 flare, the intrinsic properties of the GW190412 merger event and the properties of the host AGN of the J143041.67+355703.8 candidate flare both support a common origin for them.

The theoretical interpretation of the J143041.67+355703.8 flare as a flare produced by the GW190412 merger is straightforward. From the observed light-curve amplitude ($\sim$0.5 mag) of the J143041.67+355703.8 candidate flare and its fitted duration ($\sim$27 days), the total energy released by the J143041.67+355703.8 flare is estimated to be O(10^{49} erg). An energy release of this magnitude can be explained by the same model proposed for a BBH merger-induced flare by M. J. Graham et al. (2020), in which the postmerger BH drags its bound gas to collide with the surrounding disk gas, producing optical thermal emission. The BBH corresponding to GW190521 had a total mass of $M_{\rm BBH} \sim 160\,M_{\odot}$, and its candidate flare found by M. J. Graham et al. (2020) exhibited a duration of $\sim$50 days and a total energy release of O(10^{51} erg). In the present case, the GW190412 event has a total mass of $M_{\rm BBH} \sim 40\,M_{\odot}$. Using the radiative luminosity model from M. J. Graham et al. (2020; also see B. McKernan et al. 2019), $L_{\rm bol} \propto \eta\rho M_{\rm BBH}^2 v_k^{-3}$, where η is the radiative efficiency, ρ is the gas density in the AGN disk, and v_k is the kick velocity of the BBH, the total energy released by the J143041.67+355703.8 flare can be explained by adopting parameter values similar to those used for the candidate flare associated with GW190521: $\eta \sim 0.1$, $\rho \sim 10^{-10}\,{\rm g\,cm^{-3}}$, and $v_k \sim 200\,{\rm km\,s^{-1}}$. This kick velocity lies within the constraints from LVK GW detections (J. Calderón Bustillo et al. 2022; V. Baibhav 2025).

If the J143041.67+355703.8 flare is considered a genuine EM counterpart to the GW190412 merger, the Hubble–Lemaître constant H_0 can be constrained using its host's spectroscopic redshift from DESI and the GW luminosity distance from LVK detection (here, we used the mixed skymap). Adopting a uniform prior $H_0 \in [20, 200]\,{\rm km\,s^{-1}\,Mpc^{-1}}$ and a fixed flat ΛCDM cosmology with $\Omega_M = 0.308$ in a Bayesian framework (refer to G.-P. Li & X.-L. Fan 2025c), we obtain $H_0 = 82.9^{+40.8}_{-14.5}\,{\rm km\,s^{-1}\,Mpc^{-1}}$. This central value agrees closely with the value derived from GW190412 combined with the DESI galaxy catalog (W. Ballard et al. 2023). Such consistency supports, or at a minimum does not contradict, a physical connection between the J143041.67+355703.8 flare and the GW190412 merger.

Furthermore, it is worth noting that this work and L.-G. Zhu & X. Chen (2025) employed the same statistical framework to test the spatial correlation between BBHs and AGNs, with the key distinction being that this work specifically targeted AGNs exhibiting temporally coincident flare activity. The GW190412 event, which provides the dominant support for the nonzero most probable $f_{\rm flare}$ in this work, was also included in the analysis of L.-G. Zhu & X. Chen (2025). However, its contribution to favoring a nonzero fraction parameter $f_{\rm agn}$ in that work was not significant. This discrepancy primarily arises because the host AGN of the candidate flare counterpart J143041.67+355703.8 associated with GW190412 in this work was identified from the Milliquas (E. W. Flesch 2023) and DESI (DESI Collaboration et al. 2025) AGN catalogs, but was not recorded in the Sloan Digital Sky Survey AGN catalog (see B. W. Lyke et al. 2020 or Q. Wu & Y. Shen 2022) used by L.-G. Zhu & X. Chen (2025).

In conclusion, our search for candidate flares associated with the GWTC-4.0 BBH events, together with statistical constraints on the flare fraction parameter $f_{\rm flare}$, provides preliminary indications that a fraction of BBH mergers may be linked to ZTF flares. We caution that the nonzero estimate of $f_{\rm flare}$ is driven primarily by GW190412. Furthermore, the light curves of GW190412's sole candidate flare contain merely a single data point in each of the g and r bands during the peak period, which does not meet the criteria for inclusion in the refined AGN flare sample (such as AGNFRC) and thus it can only be regarded as a candidate. However, within the context of current nondetections of EM counterparts to BBH mergers (e.g., C. Cai et al. 2021; J. Kim et al. 2021; O. Adriani et al. 2022; S. Biswas et al. 2023; R. Poggiani 2024; G. Waratkar et al. 2024; P. Darc et al. 2025; H. Zhang et al. 2025; L. He et al. 2026; also see the "LVK GW" page in TNS for centralized reporting, https://www.wis-tns.org/ligo/events), these preliminary indications strengthen the motivation for continued counterpart searches and offer a reference for future search strategies. Clearly, establishing definitive associations—both statistical and individual—between BBH events and candidate flares remains a key objective. With the ongoing operations of the LVK network (LVK Collaboration 2025a) and the advent of new time-domain surveys such as the Wide Field Survey Telescope (T. Wang et al. 2023; S. Huang et al. 2024), the Vera C. Rubin Legacy Survey of Space and Time (LSST Science Collaboration et al. 2009; K. M. Hambleton et al. 2023), and the Einstein Probe (W. Yuan et al. 2025), it is expected that the connection between BBH mergers and their potential EM counterparts will become increasingly clear.

Acknowledgments

The authors thank Zheng-Yan Liu, Shifeng Huang, Yibo Wang, Ken Chen, Rui Niu, Yin-Jie Li, Tong Chen, Guo-Peng Li, and Chengjie Fu for helpful discussions. This work is

supported by the National Natural Science Foundation of China (grant Nos. 12325301, 12273035, 12473037), Strategic Priority Research Program of the Chinese Academy of Science (grant No. XDB0550300), the National Key R&D Program of China (grant Nos. 2021YFC2203102, 2022YFC2204602, 2024YFC2207500), the Science Research grants from the China Manned Space Project (grant No. CMS-CSST-2021-B01), the 111 Project for "Observational and Theoretical Research on Dark Matter and Dark Energy" (grant No. B23042), Cyrus Chun Ying Tang Foundations and Guizhou Provincial Major Scientific and Technological Program XKBF (2025) 011.

Software: numpy (S. van der Walt et al. 2011), scipy (P. Virtanen et al. 2020), ligo.skymap (LIGO Scientific Collaboration 2024), LALSuite (LIGO Scientific Collaboration 2018), astropy (Astropy Collaboration et al. 2013, 2018, 2022), alphashape (K. Barron 2020), pyqsofit (H. Guo et al. 2018; Y. Shen et al. 2019; W. Ren et al. 2024), matplotlib (J. D. Hunter 2007), seaborn (M. L. Waskom 2021).

Appendix
Spectrum of the Host AGN of J143041.67+355703.8

In this appendix, we present the observer-frame DESI spectrum of the host AGN of J143041.67+355703.8 (DESI Collaboration et al. 2025) (the sole candidate flare for the GW190412 merger) in Figure 4. Vertical dotted lines mark the positions of its characteristic emission or absorption lines. The mass of the central massive black hole is estimated from the width of the AGN's broad emission lines, combined with the empirical radius–luminosity relation of the broad-line region. In this work, we derive the mass of the massive black hole using the radius–luminosity relation at 5100 Å.

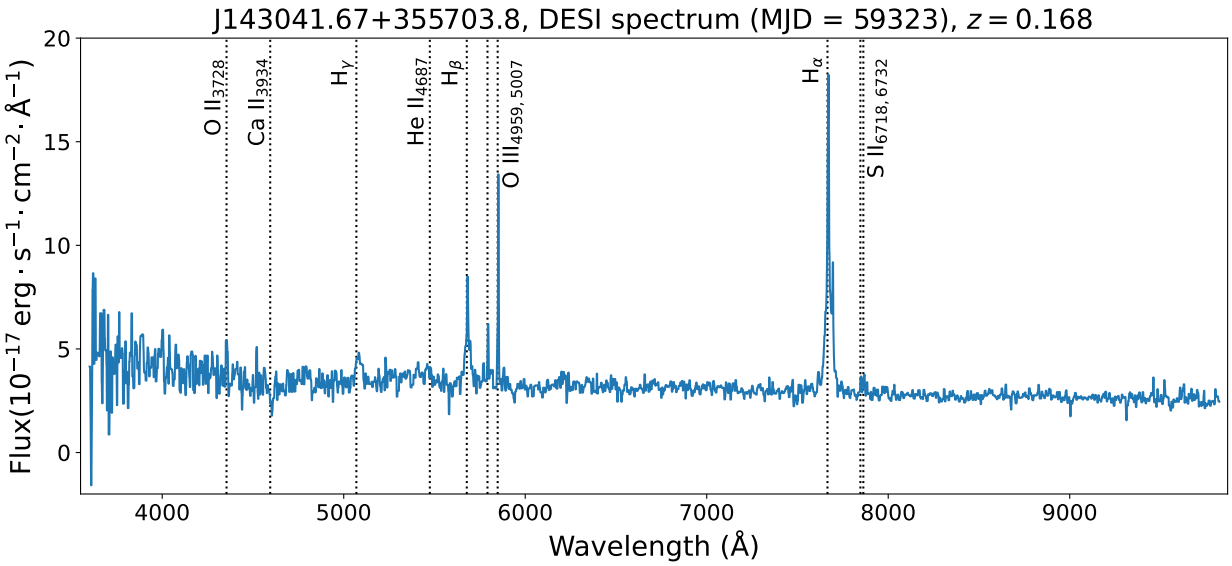

Figure 4. DESI spectrum of the host AGN of the J143041.67+355703.8 flare. Vertical dotted lines mark the positions of characteristic AGN emission or absorption lines.

ORCID iDs

Liang-Gui Zhu (朱良贵) https://orcid.org/0000-0001-7688-6504
Lei He (贺雷) https://orcid.org/0000-0001-7613-5815
Xian Chen (陈弦) https://orcid.org/0000-0003-3950-9317
Wen Zhao (赵文) https://orcid.org/0000-0002-1330-2329

References

Abac, A. G., Abouelfettouh, I., Acernese, F., et al. 2025a, ApJL, 995, L18
Abac, A. G., Abouelfettouh, I., Acernese, F., et al. 2025b, ApJL, 993, L25
Abac, A. G., Abouelfettouh, I., Acernese, F., et al. 2025c, ApJL, 993, L21
Abbott, B. P., Abbott, R., Abbott, T. D., et al. 2016, PhRvL, 116, 241102
Abbott, B. P., Abbott, R., Abbott, T. D., et al. 2019a, PhRvX, 9, 031040
Abbott, B. P., Abbott, R., Abbott, T. D., et al. 2019b, ApJL, 882, L24
Abbott, R., Abbott, T. D., Abraham, S., et al. 2020a, ApJL, 900, L13
Abbott, R., Abbott, T. D., Abraham, S., et al. 2020b, PhRvD, 102, 043015
Abbott, R., Abbott, T. D., Abraham, S., et al. 2020c, PhRvL, 125, 101102
Abbott, R., Abbott, T. D., Abraham, S., et al. 2021, PhRvX, 11, 021053
Abbott, R., Abbott, T. D., Acernese, F., et al. 2023, PhRvX, 13, 041039
Abbott, R., Abbott, T. D., Acernese, F., et al. 2024, PhRvD, 109, 022001
Ade, P. A. R., Aghanim, N., Arnaud, M., et al. 2016, A&A, 594, A13
Adriani, O., Akaike, Y., Asano, K., et al. 2022, ApJ, 933, 85
Antonini, F., Gieles, M., & Gualandris, A. 2019, MNRAS, 486, 5008
Antonini, F., & Rasio, F. A. 2016, ApJ, 831, 187
Astropy Collaboration, Price-Whelan, A. M., Lim, P. L., et al. 2022, ApJ, 935, 167
Astropy Collaboration, Price-Whelan, A. M., Sipőcz, B. M., et al. 2018, AJ, 156, 123
Astropy Collaboration, Robitaille, T. P., Tollerud, E. J., et al. 2013, A&A, 558, A33
Bagui, E., Clesse, S., De Luca, V., et al. 2025, LRR, 28, 1
Baibhav, V. 2025, arXiv:2512.22044
Ballard, W., Palmese, A., Hernandez, I. M., et al. 2023, RNAAS, 7, 250
Banerjee, S. 2017, MNRAS, 467, 524
Barron, K. 2020, alphashape: Alpha shapes in Python, 1.3.1, https://github.com/bellockk/alphashape
Bartos, I., Haiman, Z., Marka, Z., et al. 2017a, NatCo, 8, 831
Bartos, I., Kocsis, B., Haiman, Z., & Márka, S. 2017b, ApJ, 835, 165
Belczynski, K., Kalogera, V., & Bulik, T. 2002, ApJ, 572, 407
Bellm, E. C., Kulkarni, S. R., Barlow, T., et al. 2019, PASP, 131, 068003
Berti, E., Crescimbeni, F., Franciolini, G., et al. 2025, arXiv:2512.03152
Bethe, H. A., & Brown, G. E. 1998, ApJ, 506, 780
Biswas, S., Kostrzewa-Rutkowska, Z., Jonker, P. G., et al. 2023, MNRAS, 525, 4065
Brakke, K. A. 2005, https://kenbrakke.com/papers/downloads/3d.pdf
Braun, J., Dumm, J., De Palma, F., et al. 2008, APh, 29, 299
Cabrera, T., Palmese, A., & Fishbach, M. 2025, arXiv:2510.20767
Cabrera, T., Palmese, A., Hu, L., et al. 2024, PhRvD, 110, 123029
Cai, C., Xiong, S. L., Li, C. K., et al. 2021, MNRAS, 508, 3910
Calderón Bustillo, J., Leong, S. H. W., & Chandra, K. 2022, arXiv:2211.03465
Cantiello, M., Jermyn, A. S., & Lin, D. N. C. 2021, ApJ, 910, 94
Chen, K., & Dai, Z.-G. 2024, ApJ, 961, 206
Colpi, M., Mapelli, M., & Possenti, A. 2003, ApJ, 599, 1260
Darc, P., Bom, C. R., Kilpatrick, C. D., et al. 2025, PhRvD, 112, 063019
De Luca, V., Franciolini, G., & Riotto, A. 2025, arXiv:2508.09965
Delfavero, V., Ray, S., Cook, H. E., et al. 2025, arXiv:2508.13412
DESI Collaboration, Abdul-Karim, M., Adame, A. G., Aguado, D., et al. 2025, arXiv:2503.14745
Di Carlo, U. N., Giacobbo, N., Mapelli, M., et al. 2019, MNRAS, 487, 2947
Di Carlo, U. N., Mapelli, M., Giacobbo, N., et al. 2020, MNRAS, 498, 495
Dominik, M., Belczynski, K., Fryer, C., et al. 2012, ApJ, 759, 52
du Buisson, L., Marchant, P., Podsiadlowski, P., et al. 2020, MNRAS, 499, 5941
Fishbach, M., Holz, D. E., & Farr, W. M. 2018, ApJL, 863, L41
Flesch, E. W. 2023, OJAp, 6, 49
Fragione, G., & Kocsis, B. 2018, PhRvL, 121, 161103
Gayathri, V., Yang, Y., Tagawa, H., Haiman, Z., & Bartos, I. 2021, ApJL, 920, L42
Gerosa, D., Vitale, S., & Berti, E. 2020, PhRvL, 125, 101103
Gilbaum, S., Grishin, E., Stone, N. C., & Mandel, I. 2025, ApJL, 982, L13
Graham, M. J., Ford, K. E. S., McKernan, B., et al. 2020, PhRvL, 124, 251102
Graham, M. J., Kulkarni, S. R., Bellm, E. C., et al. 2019, PASP, 131, 078001
Graham, M. J., McKernan, B., Ford, K. E. S., et al. 2023, ApJ, 942, 99
Grishin, E., Gilbaum, S., & Stone, N. C. 2024, MNRAS, 530, 2114
Guo, H., Shen, Y., & Wang, S. 2018, PyQSOFit: Python code to fit the spectrum of quasars, Astrophysics Source Code Library
Hambleton, K. M., Bianco, F. B., Street, R., et al. 2023, PASP, 135, 105002
Hart, K., Shappee, B. J., Hey, D., et al. 2023, arXiv:2304.03791
Hawking, S. W. 1974, Natur, 248, 30
He, L., Liu, Z., Niu, R., et al. 2025a, ApJ, 990, 154
He, L., Liu, Z.-Y., Niu, R., et al. 2026, ApJS, 282, 13
He, L., Zhu, L.-G., Liu, Z.-Y., et al. 2025b, arXiv:2511.05144
Hirano, S., & Bromm, V. 2017, MNRAS, 470, 898
Hopkins, P. F., Richards, G. T., & Hernquist, L. 2007, ApJ, 654, 731
Huang, S., Jiang, N., Zhu, J., et al. 2024, ApJL, 964, L22
Hunter, J. D. 2007, CSE, 9, 90
Kim, J., Im, M., Paek, G. S. H., et al. 2021, ApJ, 916, 47
Kimura, S. S., Murase, K., & Bartos, I. 2021, ApJ, 916, 111
Kinugawa, T., Nakamura, T., & Nakano, H. 2021, MNRAS, 504, L28
Li, G.-P., & Fan, X.-L. 2025a, ApJ, 981, 177
Li, G.-P., & Fan, X.-L. 2025b, arXiv:2509.08298
Li, G.-P., & Fan, X.-L. 2025c, ApJ, 986, 61
Li, G.-P., Lin, D.-B., & Yuan, Y. 2023, PhRvD, 107, 063007
Li, Y.-J., Tang, S.-P., Gao, S.-J., Wu, D.-C., & Wang, Y.-Z. 2024a, ApJ, 977, 67
Li, Y.-J., Tang, S.-P., Xue, L.-Q., & Fan, Y.-Z. 2025a, ApJ, 999, 127
Li, Y.-J., Wang, Y.-Z., Tang, S.-P., Chen, T., & Fan, Y.-Z. 2025b, ApJ, 987, 65
Li, Y.-J., Wang, Y.-Z., Tang, S.-P., & Fan, Y.-Z. 2024b, PhRvL, 133, 051401
Li, Y.-J., Wang, Y.-Z., Tang, S.-P., & Fan, Y.-Z. 2025c, arXiv:2509.23897
LIGO Scientific Collaboration 2018, LIGO Algorithm Library - LALSuite, free software (GPL),
LIGO Scientific Collaboration 2024, Localization of gravitational-wave transients - ligo.skymap, 2.1.0., https://lscsoft.docs.ligo.org/ligo.skymap/index.html
Liu, B., & Lai, D. 2021, MNRAS, 502, 2049
Liu, S., Wang, L., Tanikawa, A., Wu, W., & Fujii, M. S. 2025, ApJL, 993, L30
Loredo, T. J. 2004, AIPC, 735, 195
LSST Science Collaboration, Abell, P. A., Allison, J., et al. 2009, arXiv:0912.0201
Lucarini, V. 2009, JSP, 134, 185
LVK Collaboration 2025a, https://observing.docs.ligo.org/plan/LIGO, Virgo and KAGRA observing run plans
LVK Collaboration, Abac, A. G., Abouelfettouh, I., Acernese, F., et al. 2025b, arXiv:2508.18082
LVK Collaboration, Abac, A. G., Abouelfettouh, I., Acernese, F., et al. 2025c, arXiv:2508.18083
Lyke, B. W., Higley, A. N., McLane, J. N., et al. 2020, ApJS, 250, 8
Mandel, I., Farr, W. M., & Gair, J. R. 2019, MNRAS, 486, 1086
Mapelli, M. 2021, in Handbook of Gravitational Wave Astronomy, ed. C. Bambi, S. Katsanevas, & K. D. Kokkotas, 16 (Springer)
Mapelli, M., Dall'Amico, M., Bouffanais, Y., et al. 2021, MNRAS, 505, 339
McKernan, B., Ford, K. E. S., Bartos, I., et al. 2019, ApJL, 884, L50
McKernan, B., Ford, K. E. S., Lyra, W., & Perets, H. B. 2012, MNRAS, 425, 460
Miller, M. C., & Hamilton, D. P. 2002, MNRAS, 330, 232
Okabe, A., Boots, B., & Sugihara, K. 2000, Spatial Tessellations: Concepts and Applications of Voronoi Diagrams (Wiley)
Olejak, A., Fishbach, M., Belczynski, K., et al. 2020, ApJL, 901, L39
Palmese, A., Fishbach, M., Burke, C. J., Annis, J., & Liu, X. 2021, ApJL, 914, L34
Passenger, L., Banagiri, S., Thrane, E., et al. 2025, arXiv:2510.14363
Poggiani, R. 2024, AnP, 536, 2200215
Postnov, K. A., & Yungelson, L. R. 2014, LRR, 17, 3
Ren, W., Guo, H., Shen, Y., et al. 2024, ApJ, 974, 153
Rodriguez, C. L., Chatterjee, S., & Rasio, F. A. 2016, PhRvD, 93, 084029
Rodriguez, C. L., Kremer, K., Grudić, M. Y., et al. 2020, ApJL, 896, L10
Rodriguez, C. L., Morscher, M., Pattabiraman, B., et al. 2015, PhRvL, 115, 051101
Rodríguez-Ramírez, J. C., Bom, C. R., Fraga, B., & Nemmen, R. 2024, MNRAS, 527, 6076
Samsing, J., Bartos, I., D'Orazio, D. J., et al. 2022, Natur, 603, 237
Santoliquido, F., Mapelli, M., Giacobbo, N., Bouffanais, Y., & Artale, M. C. 2021, MNRAS, 502, 4877
Secunda, A., Bellovary, J., Mac Low, M.-M., et al. 2020, ApJ, 903, 133
Shen, X., Hopkins, P. F., Faucher-Giguère, C.-A., et al. 2020, MNRAS, 495, 3252
Shen, Y., Hall, P. B., Horne, K., et al. 2019, ApJS, 241, 34
Stacy, A., Greif, T. H., & Bromm, V. 2010, MNRAS, 403, 45

Tagawa, H., Haiman, Z., Bartos, I., & Kocsis, B. 2020a, ApJ, 899, 26
Tagawa, H., Haiman, Z., & Kocsis, B. 2020b, ApJ, 898, 25
Tagawa, H., Kocsis, B., Haiman, Z., et al. 2021, ApJ, 908, 194
Tanikawa, A., Liu, S., Wu, W., Fujii, M. S., & Wang, L. 2025, arXiv:2508.01135
Thrane, E., & Talbot, C. 2019, PASA, 36, e010
Tonry, J. L., Denneau, L., Heinze, A. N., et al. 2018, PASP, 130, 064505
van der Walt, S., Colbert, S. C., & Varoquaux, G. 2011, CSE, 13, 22
Vavilova, I., Elyiv, A., Dobrycheva, D., & Melnyk, O. 2021, in Intelligent Astrophysics, ed. I. Zelinka, M. Brescia, & D. Baron, Vol. 39 (Springer), 57
Veronesi, N., Rossi, E. M., & van Velzen, S. 2023, MNRAS, 526, 6031
Veronesi, N., Rossi, E. M., van Velzen, S., & Buscicchio, R. 2022, MNRAS, 514, 2092
Veronesi, N., van Velzen, S., & Rossi, E. M. 2024, MNRAS, 536, 3112
Veronesi, N., van Velzen, S., Rossi, E. M., & Storey-Fisher, K. 2025, MNRAS, 536, 375
Virtanen, P., Gommers, R., Oliphant, T. E., et al. 2020, NatMe, 17, 261
Voronoi, G. 1908, JRAM , 1908, 198
Wang, J.-M., Liu, J.-R., Ho, L. C., Li, Y.-R., & Du, P. 2021a, ApJL, 916, L17
Wang, T., Liu, G., Cai, Z., et al. 2023, SCPMA, 66, 109512
Wang, Y.-Z., Fan, Y.-Z., Tang, S.-P., Qin, Y., & Wei, D.-M. 2021b, arXiv:2110.10838
Wang, Y.-Z., Li, Y.-J., Vink, J. S., et al. 2022, ApJL, 941, L39
Waratkar, G., Bhalerao, V., & Bhattacharya, D. 2024, ApJ, 976, 123
Waskom, M. L. 2021, JOSS, 6, 3021
Woosley, S. E. 2016, ApJL, 824, L10
Wu, Q., & Shen, Y. 2022, ApJS, 263, 42
Yang, Y., Bartos, I., Gayathri, V., et al. 2019b, PhRvL, 123, 181101
Yang, Y., Bartos, I., Haiman, Z., et al. 2019a, ApJ, 876, 122
Yuan, W., Dai, L., Feng, H., et al. 2025, SCPMA, 68, 239501
Zevin, M., Bavera, S. S., Berry, C. P. L., et al. 2021, ApJ, 910, 152
Zhang, H., Kokubo, M., MacBride, S., et al. 2025, arXiv:2508.00291
Zhu, L.-G., & Chen, X. 2025, ApJL, 989, L15
Ziosi, B. M., Mapelli, M., Branchesi, M., & Tormen, G. 2014, MNRAS, 441, 3703